# DESIGN AND CHARACTERIZATION OF COLD POINT THERMOELECTRIC COOLERS

Uttam Ghoshal

NanoCoolers Inc., Austin, TX 78746; e-mail:ghoshal@nanocoolers.com
Research performed in part at IBM Research, Austin Research Laboratory, Austin, TX 78758.

## Abstract

We describe structured point-contact thermoelectric devices that confine the thermal gradients and electric fields at the boundaries of the cold end, and exploits the reduction of thermal conductivity at the interfaces, tunneling properties of point contacts, and the poor electron-phonon coupling at the junctions. We propose a theory of the structured cold point metal-semiconductor contacts and detail the design of cold point thermoelectric coolers. Temperature and electrical measurements of prototype cold point coolers using bismuth chalcogenides in vacuum indicate doubling of the thermoelectric figure-of-merit *ZT* values to the range of 1.4-1.7 at room temperature.

## Introduction

Solid-state thermoelectric coolers can revolutionize thermal management of electronics and optoelectronic systems, and small-scale refrigeration if the coolers could attain thermodynamic efficiency greater than 30% of the ideal Carnot cycle. The maximum temperature differential and the efficiency of thermoelectric coolers are known to depend on material properties through the thermoelectric figure-of-merit $ZT = S^2\sigma T/\lambda$. $Z$ has units of inverse temperature, and depends on the Seebeck coefficient $S$, the electrical conductivity $\sigma$, the thermal conductivity $\lambda$. The efficiency requirements imply the figure-of-merit needs to be increased from $ZT \sim 1$ typical of bismuth chalcogenides at room temperatures to $ZT > 3$. The cooling power per unit area is primarily dependent on the critical transport length of the thermoelement and can easily exceed 50W/cm$^2$ in thin-film cooler structures [1]. A variety of promising approaches such as transport and confinement in nanowires and quantum dots, reduction of thermal conductivity in the direction perpendicular to superlattice planes, and optimization of ternary or quaternary chalcogenides and skutteridites have been investigated recently [2,3].

## Theory

We have been investigating the scaling properties of thin-film thermoelectric coolers, and the properties of structured point contacts at the cold end [4]. In these structured cold point thermoelectric coolers (Fig.1a), the electric field and temperature gradients are localized within distances of the order of the individual tip radius $r_0$ if the interface and spreading electrical and thermal resistances are much larger than the bulk (body) resistance of the thermoelements. It can be shown that a conservative criterion is $p > \sqrt{2\pi r_0 t}$ , $p$ being the distance between the points and $t$ the thickness of the thermoelements. The microscopic structure of the point contacts varies between the two extreme scenarios depicted in Fig.1b. In one extreme, the contact is primarily by electronic tunneling through a gap wherein the phonon coupling via near-field coupling is negligible. In the other extreme, the metal tip compresses the surface of the thermoelement and the transport is dependent on both electronic tunneling and phonon conduction.

When an electronic current $I$ is injected through the tunneling cold point contact (corresponding to the first scenario, with processes described in Fig. 2), the heat flow/temperature relations can be obtained by considering purely electronic conduction by tunneling processes in the gap and a two-fluid electron-phonon conduction in the semiconductor *Sm* with Seebeck coefficient $S_0$. If $q_e(r_0)$ represents the electronic heat flow into the surface of the semiconductor *Sm*, the overall heat balance relations in the tunneling region can be written as follows:

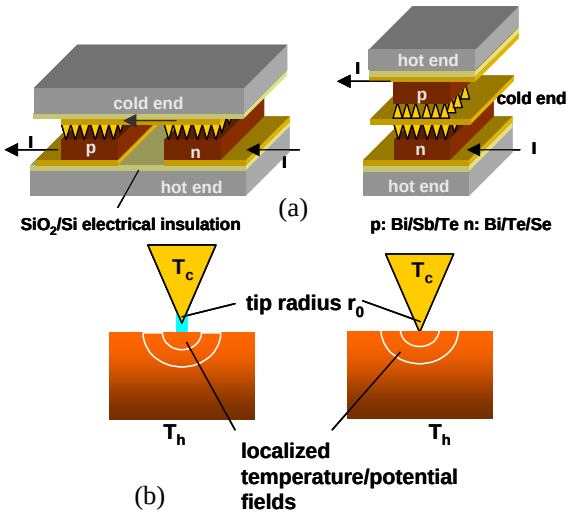


Fig.1(a) Vertical and lateral structured cold end thermoelectric coolers (b) Schematic illustration of two limiting cases for operation of a cold point contact with tip radius $r_0$: first, the electronic tunneling regime with negligible phonon conduction, and second, the case where tip is in physical contact with the surface and there is a finite phonon conduction.

$$q_0 = P_{mt} + P_{ts} - P_{Jm} - P_{Jt} + q_e(r_0) \quad ...(1)$$

If $S_t$ represents the Seebeck coefficient in the tunneling region, $P_{mt} = S_t I T_c$ and $P_{ts} = (S_0 - S_t) I T_e(r_0)$. The Joule heating in the metal tip, $P_{Jm} \approx I^2/(\varphi\sigma_m r_0)$ where $s_m$ is the electrical conductivity of the metal *M*, and $\varphi$ is the solid-angle subtended by of the conical tip [5]. ($\varphi = \pi$ when the half-angle of the cone is 45°). The Joule heating resulting from the tunneling process $P_{Jt} = I^2 R_t$. Hence equation (1) can be written as:

$$q_0 = [S_t T_c + (S_0 - S_t) T_e(r_0)] I - I^2 [R_t + 1/(\varphi\sigma_m r_0)] + q_e(r_0) \quad ...(2)$$

Heat flow balance at the cold end node requires,

$$q_0 = P_{mt} - P_{Jm} - P_{Jt}/2 - K_t [T_e(r_0) - T_c] \quad ...(3)$$

In the above relation, we have assumed that half of the Joule dissipation in the tunneling region flows back to the cold end. This is a conservative estimate for the cooling power $q_0$ because electrons tend to deposit a larger fraction of the Joule heat at the receiving semiconductor end [5]. We can use equation (3) to express $T_e(r_0)$ in terms of the cold end temperature $T_c$ and the cooling power $q_0$:

$$T_e(r_0) = \left[1 + \frac{S_t I}{K_t}\right] T_c - \frac{q_0}{K_t} - \frac{I^2 R_t}{2K_t} - \frac{I^2}{\varphi\sigma_m r_0 K_t} \quad ...(4)$$

The three tunneling parameters: zero-current electronic thermal conductance $K_t$, the tunneling resistance $R_t$, and the Seebeck coefficient $S_t$, are strongly dependent on the tunneling gap $\delta_t$ between the tip and the semiconductor, and the energy barrier height $V_b$ at the interface [6]. If we define $\delta_0$ as the decay length for the tunneling process, the equivalent Mott's expression for the Seebeck coefficient $S_t$ has the form:

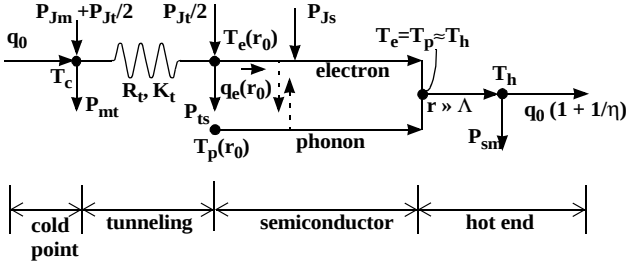


Fig.2 Thermal heating and cooling processes in the cold point structure. $P_{mt}$ and $P_{ts}$ denote the Peltier cooling at the metal tip and semiconductor surface respectively, while $P_{sm}$ denotes the Peltier heat released at the distant semiconductor-metal boundary. $P_{Jm}$, $P_{Jt}$ and $P_{Js}$ represent the Joule heating in the metal tip, tunneling region, and the semiconductor respectively. $K_t$ and $R_t$ represent the zero-current thermal conductance and tunneling resistance of the tunneling region. The electrons and the phonon systems have different temperatures ($T_e(r_0)$ and $T_p(r_0)$) near the surface of the semiconductor but are in equilibrium at distances $r \gg L$. $q_0$ denotes the cooling power at the cold end and $h$ is the coefficient of performance for the single cold point cooling structure.

$$S_t = \left(\frac{\pi^2}{3}\right)\left(\frac{k_B}{e}\right)\left(\frac{k_B T_c}{V_b}\right)\left(\frac{\delta_t}{\delta_0}\right) \quad ...(5)$$

The tunneling resistance $R_t$ for a cross sectional area $\pi r_0^2$ has the generic form:

$$R_t = \frac{r^*}{r_0^2}\left(\frac{\delta_t}{\delta_0}\right)\exp\left(\frac{2\delta_t}{\delta_0}\right) \quad ...(6)$$

where $r^*$ is a parameter that can be extracted from measurements, and is dependent on local density-of-states and the direct or indirect phonon-assisted nature of tunneling. The zero-current electronic thermal conductance $K_t$ can be derived from the relation:

$$K_t = \frac{(L_0 - S_t^2) T_c}{R_t} \quad ...(7)$$

where $L_0 = (\pi^2/3)(k_B/e)^2 = (156\ \mu V/K)^2$ is the Lorentz number for ballistic transmission. Note that the above relations for the tunneling parameters are derived under the assumption $k_B T_c \ll V_b(\delta_0/\delta_t)$ that implies $S_t^2 < L_0$. Also note that the band gaps and the barrier heights $V_b$ for the thermoelectric materials of interest such as $Bi_2Te_3$ and InSb are small i.e. of the order of 6-8 $k_B T_c$.

The electrons injected into the semiconductor *Sm* are not in thermal equilibrium with the phonon system for a finite distance $\Lambda$ from the surface. The coupled equations for heat transfer for the electron-phonon system near the surface within the semiconductor *Sm* are:

$$P(T_e - T_p) - \nabla\bullet(\lambda_e \nabla T_e) - \frac{|J|^2}{\sigma} = 0 \quad ...(8)$$

$$P(T_p - T_e) - \nabla\bullet(\lambda_{sp} \nabla T_p) = 0$$

where the parameter *P* represents the intensity of the electron-phonon interaction [6,7], *J* is the local current density, $T_e$ and $T_p$ denote the electron temperature and phonon temperature respectively, $\sigma$ is the electrical conductivity, $\lambda_e$ is the electronic thermal conductivity, and $\lambda_{sp}$ is the surface lattice thermal conductivity. We have solved the radially-symmetric coupled equations (8) subject to zero phonon-based heat conduction $\lambda_{sp} dT_p/dr = 0$ at the surface, and the constraint $T_e(r), T_p(r) \to T_h$ at large distances from the point contact. The solution indicates that the characteristic thermalization length $\Lambda$ can be expressed as $\Lambda = \sqrt{\lambda_e \lambda_{sp}/[(\lambda_e + \lambda_{sp})P]}$ and the nonequilibrium effects result in a reduced thermal conductivity $\lambda$ at the point contact:

$$\lambda = \frac{\lambda_e(1 + r_0/\Lambda)(1 + \lambda_e/\lambda_{sp})}{1 + (\lambda_e/\lambda_{sp})(1 + r_0/\Lambda)} \quad (9)$$

As $r_0/\Lambda \to \infty$, $\lambda \to \lambda_{sp} + \lambda_e$ and as $r_0/\Lambda \to 0$, $\lambda \to \lambda_e$. The characteristic thermalization length $\Lambda$ is about 300 nm for our material system. The heat flow $q_e(r_0)$ can be expressed in terms of $T_e(r_0)$, $T_h$, and the current *I*:

$$q_e(r_0) = -\theta r_0 \lambda (T_h - T_e(r_0)) - \frac{I^2}{2\theta\sigma r_0}\xi \quad ...(10)$$

The back-flow of Joule heat from the semiconductor *Sm* to the cold end is reduced by a factor $\xi$ given by:

$$\xi = 1 - \left(\frac{r_0/\Lambda}{1+(\lambda_e/\lambda_p)(1+r_0/\Lambda)}\right)\left(1+\frac{r_0}{\Lambda}e^{r_0/\Lambda}Ei(-r_0/\Lambda)\right) \quad ...(11)$$

We can use equations (4) and (11) to eliminate $T_e(r_0)$ and $q_e(r_0)$ from equation (2), and express the cooling power $q_0$ in terms of $T_c$, $T_h$, and the current $I$:

$$q_0 = \frac{1}{1+[\theta r_0\lambda + (S_0 - S_t)I]/K_t}\left\{ I\left[S_0T_c + \frac{IS_tT_c(S_0-S_t)}{K_t} - I^2\left(\frac{R_t}{2}+\frac{1}{\varphi\sigma_m r_0}\right)\frac{S_0-S_t}{K_t}\right] - I^2\left[R_t + \frac{1}{\varphi\sigma_m r_0} + \frac{\xi}{2\theta\sigma r_0}\right] - \theta r_0\lambda\left[T_h - T_c - \frac{S_tT_cI}{K_t} + \frac{I^2}{K_t}\left(\frac{R_t}{2}+\frac{1}{\varphi\sigma_m r_0}\right)\right]\right\} \quad ...(12)$$

The electrical power supplied by the external source is simply the total power $Q$ dissipated in the system:

$$Q = I^2\left(R_t + \frac{1}{\varphi\sigma_m r_0} + \frac{1}{\theta\sigma r_0}\right) + S_t(T_e(r_0) - T_c)I + S_0(T_h - T_e(r_0))I \quad ...(13)$$

or,

$$Q = I^2\left(R_t + \frac{1}{\varphi\sigma_m r_0} + \frac{1}{\theta\sigma r_0}\right) + S_0I(T_h - T_c) - \frac{(S_0-S_t)}{K_t}\left[q_0 + I^2\left(\frac{R_t}{2}+\frac{1}{\varphi\sigma_m r_0}\right) - S_tT_cI\right] \quad ...(14)$$

The coefficient of performance (COP) of a single point cooler is $\eta = q_0/Q$ .The thermodynamic efficiency $\varepsilon_p$ of the cooling process at a single cold point in the first scenario of Fig. 1b can be calculated from the relation:

$$\varepsilon_p = \left(\frac{T_h - T_c}{T_c}\right)\frac{q_0}{Q} \quad ...(15)$$

In the other extreme scenario of Fig. 1b, the metal tip compresses the surface of the thermoelement and the transport is dependent on both electronic tunneling and phonon conduction. The finite heat conduction by phonons at the tip results in lowering of the phonon temperature at the surface, and $\lambda \approx \lambda_{sp} + \lambda_e$ . Note that the surface lattice thermal conductivity $\lambda_{sp}$ is lower than the bulk thermal conductivity due to Kapitza boundary effects and less understood pressure/stress effects that affect phonon scattering at point contacts. Pressure effects could also increase the local Seebeck coefficients in p-type $Bi_{0.5}Sb_{1.5}Te_3$ [9].

We have also analyzed the effects of few-molecular-layer thermoelectric overcoats over the metal tips, and the effect of finite phonon conduction at the tip. These results are beyond the scope of this paper and will be published elsewhere. Fig. 3 shows the numerically modelled performance of $Bi_2Te_{2.8}Se_{0.2}$ point junctions as a function of the tip radius and the tip-surface separation that indicate $ZT \sim 3$.

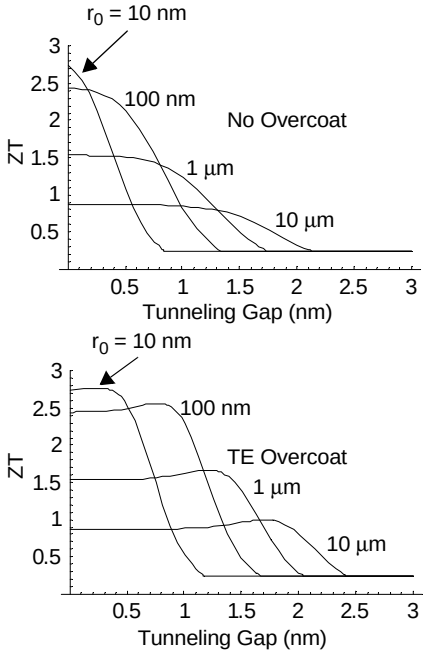


Fig.3 Numerically modelled performance of metal-$Bi_2Te_{2.8}Se_{0.2}$ point junctions as a function of tip radius $r_0$ and the tunnelling gap $\delta_t$. Thermoelectric overcoats on the tips can reduce the dependency of $ZT$ on the tip-surface separation.

**Design Considerations**

The design of the cold point coolers are similar to that of conventional thermoelectric coolers. In order to match the I-V characteristics of the cold point thermoelectric coolers to the characteristics of the dc supply source, we need to group $N_p$ cold points per (n-type or p-type) thermoelement such that the total current through the $\sqrt{N_p}\times\sqrt{N_p}$ array equals the design-specified maximum source current $I_m$, and the COP meets the application requirements (say, $\eta = \eta_0$). Each group of cold points in a thermoelement is electrically connected in series to complementary thermoelements at the cold end and the hot end using metal links of thickness $t_m$. The spacing between the thermoelements can be small compared to the dimensions of the cold point array, so that the link resistance $R_l$ equals two squares of sheet resistance i.e., $R_l = 2/(\sigma_m t_m)$. The reduction in cooling power per cold point due to the link resistance is $q_{Jl} = I_m^2/(\sigma_m t_m N_p)$, while the additional power required from the external source equals $2q_{Jl}$. If the cold point coolers operate in partial vacuum between specified cold end and hot end temperatures, the number $N_p$ is obtained by solving the relation:

$$\frac{q_0(I_m/N_p, T_c, T_h) - I_m^2/(\sigma_m t_m N_p)}{Q(I_m/N_p, T_c, T_h) + 2I_m^2/(\sigma_m t_m N_p)} = \eta_0 \quad ...(16)$$

The number of thermoelements $N_t$ that need to be connected in the electrically-series, thermally parallel circuit to produce a total cooling power $Q_0$ is $N_t = Q_0/(N_p q_0)$ The total voltage $V_t$ across the QCP cooler that cools $Q_0$ watts at a COP = $\eta_0$ is given by $V_t = Q_0/(\eta_0 I)$ .

## Measurements

We have recently fabricated and measured the temperature-current and voltage-current characteristics of a prototype cold point thermoelectric cooler based on a p-type $Bi_{0.5}Sb_{1.5}Te_3$ and n-type $Bi_2Te_{2.9}Se_{0.1}$ material system [10]. The cold point coolers operated in vacuum (~3 mTorr) bell jar housing a two-axis micrometer. The heat load at the cold end consisted of conduction loss due to the two leads of the thermocouple and radiation loss due to a thermocouple leads and a peripheral overhang. Fig. 4a shows the typical maximum temperature differential-current and four-point voltage-current data for an 80 × 80 array of cold points at a pitch of 20 μm with tip radius of 0.6 μm. A nonlinear curve fit to the Δ*T*-*I* and *V*-*I* data resulted in $ZT_a$ = 1.4. At low current density and smaller temperature differentials, the coolers operate at thermodynamic efficiency of 17-21% — significantly better than conventional ones. We do not yet fully understand the factors that limit the temperature differential in the cold point coolers to 70-75K at high currents. Fig. 4a also compares the performance of the cold point coolers to a 2-element thermoelectric cooler fabricated by Marlow Industries, Inc. and tested in the same setup under similar conditions. The length of the Marlow thermoelements was 1.52 mm and the cross section area was 0.63×0.63 mm$^2$. The intrinsic $Z_iT_a$ discounting the effects of heat loading was measured by another independent experiment that exploited the fact that thermal conduction by air suppresses the cooling effects in arrays with low density of cold points. The differential electrical resistance for small currents is given by,

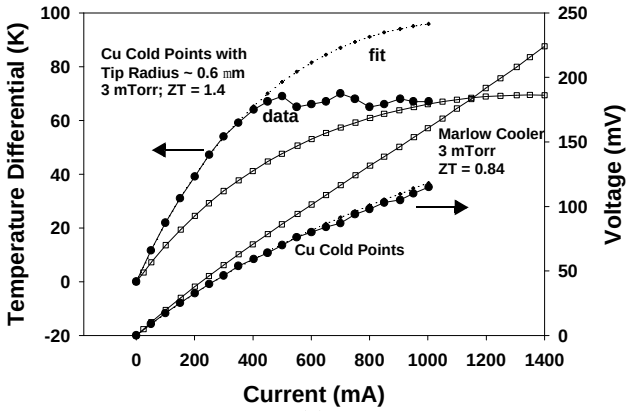


(a)

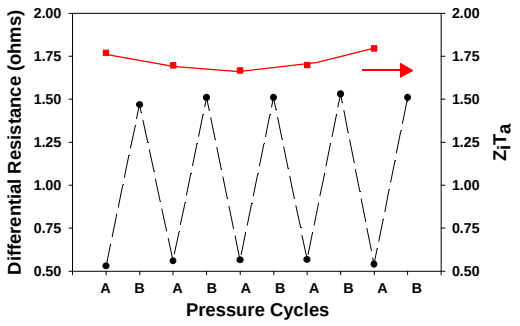


(b)

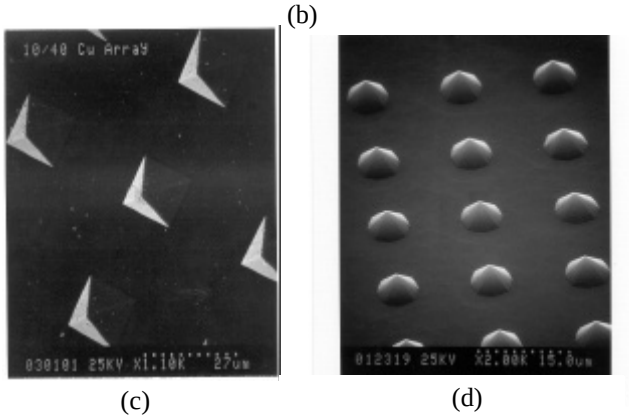

(c) (d)

Fig.4 (a) Performance of cold point thermoelectric coolers with pyramidal all-metal points (c). (b) Direct determination of *intrinsic* $Z_iT_a$ ~ 1.7 by measuring the differential resistance at small currents in vacuum and in ambient. (d) Alternative Si-based cold point structures with thermoelectric overcoats

$$\partial V/\partial I|_{I\to 0} = R + S\partial\Delta T/\partial I|_{I\to 0} = R + S^2T_a/K \quad ...(17)$$

where *R*, *K*, and *S* represent the total electrical resistance, the total thermal conductance, and the net Seebeck coefficient of the prototype cooler. For a sparse array in which thermal conduction by air is the dominant contributor to *K*, the differential resistance for small currents is simply the ohmic resistance *R*. Hence in such cases,

$$Z_iT_a = (\partial V/\partial I|_{vacuum} - \partial V/\partial I|_{air})/(\partial V/\partial I|_{air}) \quad ...(18)$$

Fig. 4b shows the differential resistance at low currents and the $Z_iT_a$ extracted from a cold point cooler with a 40 × 40 array of cold points at a pitch of 40 μm subjected to pressure cycles between ambient atmospheric pressure and vacuum, with an optimized adjustment of the micrometer. The cold end structure did not include the thermocouple or the overhang, and minimized the radiation parasitics. $Z_iT_a$ ~ 1.7 measured by this method agrees well with the estimates for parasitics in the Δ*T*-*I* and *V*-*I* experiments. Reference [10] discusses the experiments in greater detail.

## Conclusions

We have presented the first-order design and the Δ*T*-*I* and *V*-*I* characterization of prototype cold point thermoelectric device structures. The preliminary experiments indicate doubling of thermodynamic efficiencies of coolers with bismuth chalcogenides. The cold point thermoelectric coolers promise enhanced figure-of-merit $ZT \sim \pi$ in ideal point configurations.

## References


[1] U. Ghoshal and R. Schmidt, ISSCC Dig.Tech., **43**, 216, (2000).
[2] F. J. DiSalvo, Science, **285**, 703 (1999).
[3] R. Venkatasubramanian *et al.*, Nature, **413**, 597 (2001).
[4] Y. S. Ju and U. Ghoshal, J. Appl. Phys., **88**, 4135 (2000).
[5] J. B. Xu *et al.*, Appl. Phys. **A 59**, 155, (1994).
[6] M. Bartkowiak and G. Mahan, Mat. Res. Soc. Symp. Proc., **545**, 265 (1999).
[7] V. Zakordonets and G. Loginov, Semiconductors, **31**, 265 (1997).
[8] B.K. Ridley, *Electrons and Phonons in Semiconductor Multilayers* (Cambridge Press, 1997) Chapter 11.
[9] D. Polvani *et al.*, Chem. Mater., **13**, 2068 (2001).
[10] U. Ghoshal *et al.*, Appl. Phys. Lett., 80, 3006 (2002).